Petroleum Science 23 (2026) 1039–1052

Contents lists available at ScienceDirect

Petroleum Science

journal homepage: www.keaipublishing.com/en/journals/petroleum-science

Original Paper

Timing of deep oil accumulations in the western part of the northern Tarim Basin: Records from fluid inclusions and carbonate U–Pb dating

Hui Zhou [a], Li-Li Gui [a,b,*], Xue-Song Lu [a,b], Xiu-Yan Chen [a], Yuan-Quan Zhou [a,b], Ying-Ying Wang [a,b], Shi-Hua Yao [a,b,c], Xiao-Qing Yu [a,b], Wen-Xia Yang [a,d]

[a] PetroChina Research Institute of Petroleum Exploration & Development, Beijing, 100083, China
[b] State Key Laboratory of Enhanced Oil Recovery, Beijing, 100083, China
[c] China University of Geosciences, Beijing, 100083, China
[d] Northwest Oilfield Branch Company, Sinopec, Urumqi, 830011, Xinjiang, China

ARTICLE INFO

Article history:
Received 16 January 2025
Received in revised form
10 June 2025
Accepted 8 September 2025
Available online 24 September 2025

Edited by Xi Zhang and Jie Hao

Keywords:
Deeply buried reservoir
Carbonate U–Pb dating
Fluid inclusion
Kalayuergun
Tarim Basin

ABSTRACT

Liquid oils in deeply buried reservoirs are usually subjected to thermal cracking by the prolonged time-temperature effect during burial. However, large quantity liquid oils are being produced from the Cambrian reservoirs in the Tarim Basin at a depth of over 5500 m. Previous studies suggest that a late oil charging event should have been responsible for the preservation of liquid oil, but the evidence from fluid inclusions is questionable. In this study, carbonate U–Pb dating following a systematic fluid inclusion analysis is applied to constrain the timing of oil charging in the Cambrian reservoir in the Kalayuergun structural belt in the western part of the Tabei Uplift. The results show that the diagenetic minerals of the Cambrian Xiaqiulitage Formation include the dolomite matrix, anhedral dolomite, euhedral dolomite and calcite. Secondary oil inclusions were detected as trails in the dolomite matrix while primary oil inclusions are distributed along growth zones of calcite. Both of these inclusions are featured by multiple fluorescence colors in single oil inclusion assemblage, which are interpreted to be the results of trapping fractionation or post-entrapment alteration. The homogenization temperatures of oil inclusions with different fluorescence colors in the same assemblage are in the same range of their coeval aqueous inclusions, denoting oil inclusions are formed in a single trapping event and the oil should have been gas saturated. Projecting the lowest homogenization temperature of the aqueous inclusion onto the burial history, yielding an age of around 450 Ma which is very close to the U–Pb age of calcite (440.5 ± 9.6 Ma), corresponding to the first oil generation peak of the Yuertusi Formation during the Late Ordovician to Early Silurian. Considering this, the early generated oils migrated upwards to the shallower reservoir through fault planes together with the low heating rate of the Tarim Basin prevented the oil in place from thermal cracking. This study demonstrates the effectiveness of integrating carbonate U–Pb dating and fluid inclusion methods to investigate deeply buried reservoirs in the Tarim Basin, which can be applied to similar reservoirs in the world.

1. Introduction

Unlike the Sinian-Cambrian deeply buried reservoirs (DBRs, burial depth >5000 m) in the Sichuan Basin (SW China) where the oils generated from marine source rocks have completely cracked to natural gas due to a high grade of thermal evolution (Dai et al., 2014; Guo et al., 2016; Xu et al., 2018; Zou et al., 2014), the Cambrian–Ordovician DBRs in the Tarim Basin that are buried down to 8 km are producing large amounts of light oils (Chai et al., 2020; Chen et al., 2019; Yang et al., 2020; Zhu et al., 2020, 2021). This has attracted petroleum geologists to understand the preservation mechanisms of the light hydrocarbons from thermal cracking in the ultra-deep context during the long geological history (Chai et al., 2020; Du and Hu, 2024; Jiang et al., 2024; Jin, 2023; Li et al., 2023; Zhang et al., 2022; Zhu et al., 2013). In this regard, determining the time of oil charging is essential, because the Tarim Basin has relatively low geothermal gradient (Liu et al., 2016). This

* Corresponding author.
E-mail address: gll@petrochina.com.cn (L.-L. Gui).
Peer review under the responsibility of China University of Petroleum (Beijing).

https://doi.org/10.1016/j.petsci.2025.09.013

means, later charges of oil should suffer less from the combined temperature-time effect making them more likely to form larger light oil accumulations to be found present-day (Zhu et al., 2020).

Biomarker-based studies have suggested the oils in present-day reservoirs of the Tarim Basin have experienced three oil charging episodes and multiple oil mixing events (Zhan et al., 2017; Zhou et al., 2021). However, other studies based on fluid inclusion analysis suggest only two oil charging episodes in the Tarim Basin (Fang et al., 2017; Xiao et al., 2016). The determination of two oil charging episodes by fluid inclusions was mainly based on two different fluorescence colors of oil inclusions that have been long considered representing oils with distinctive thermal maturities (Stasiuk and Snowdon, 1997) and a bimodal histogram of homogenization temperature of the aqueous inclusions representing two major fluid activities (Song et al., 2017). However, using the fluorescence color of oil inclusions to decide charging episodes is still questionable, since inclusions could have been subjected to various secondary processes other than thermal maturation, affecting oil inclusions' fluorescence colors (George et al., 2001b). In addition, in vein filling carbonate minerals, fluid inclusions are generally distributed either as clusters or trails, thus, it is hard to identify theoretically coeval oil and aqueous inclusions that should coexist in one fluid inclusion assemblage (FIA) (Goldstein and Reynolds, 1994). Moreover, recent progress related to fluid inclusions suggest that the size and abundance of inclusions largely affect their connectivity, consequently, primary inclusions could have been filled by secondary fluids in carbonate minerals with dense inclusions (Eltom et al., 2023). In the existing studies targeting oil charging in the Tarim Basin, the two different fluorescent oil inclusions are commonly found coexisting in single crystals, thus, making two-episode interpretations unreliable (Song et al., 2017; Yang et al., 2021a). Besides, the reported bimodal histograms of homogenization temperatures are not quite convincing, because there exists a large amount of data between the two modes on the histograms left out (Fang et al., 2017; Xiao et al., 2016). Additionally, previous studies found coeval aqueous inclusions of the second oil charging exhibit distinctively different salinity ranges between two neighboring wells of around 20 km apart, which was attributed to the differences in the hydrodynamics of two separate fluids (Yang et al., 2021a). Ultimately, all of the reported aqueous inclusion data could be problematic in carbonate crystals.

In-situ U–Pb dating is a powerful method for geochronology (Gui et al., 2025; Jackson et al., 2004). The development of a calcite reference material WC-1 (Roberts et al., 2017) has facilitated carbonate in-situ U–Pb dating, particularly in the oil and gas industry as carbonate is the most common mineral type in diagenetic regimes (Cong et al., 2021; Gui et al., 2023; Lu et al., 2023; Yang et al., 2021b). The absolute age of diagenetic minerals can eliminate the ambiguity introduced by fluid inclusion-burial history indirect dating, so, minimize the uncertainty in the timing of paleofluids activities, providing better constraints on oil/gas charging histories especially in superimposed basins with complex tectonic backgrounds (Cong et al., 2024; Liu et al., 2022; Su et al., 2022). For example, Fan et al. (2023) employed in-situ U–Pb dating of carbonate veins in Cambrian shales at the southeastern margin of the Upper Yangtze platform (SW China) to constrain fluid and hydrocarbon activities in shales. Mangenot et al. (2018) coupled carbonate U–Pb dating and clumped isotope thermometry and calibrated the thermal history of the Middle Jurassic carbonates in the Paris Basin (France). Rasmussen et al. (2020) identified six fluid episodes in the Pilbara craton by applying U–Pb dating to Archean shale hosting calcite veins. Therefore, it is vital to incorporate such methods when investigating fluids in the Tarim Basin that have shown a complex geodynamic context. Cong et al. (2022) employed carbonate U–Pb dating in oil inclusions-bearing calcite in the Halahatang oilfield and obtained two main absolute ages corresponding to two major oil charging episodes. Xu et al. (2024) identified four different calcite phases in the Ordovician reservoir in the Tabei Uplift of the Tarim Basin, which then proved to have oil inclusions with different fluorescence colors, varying rare earth element (REE) abundancy patterns, distinctive stable C–O isotope distributions and four variable U–Pb ages. Therefore, these four calcite filling events attributed to four fault activities related to oil charging episodes. In another study, although, authors found three oil inclusion groups with different fluorescence colors in calcite veins and cements, the U–Pb dating results only supported the first oil charging event (Cong et al., 2024).

The Ordovician marine carbonates are the major oil reservoirs of the Tarim Basin (Xiao et al., 2016). The source of the Paleozoic marine hydrocarbons in the Tarim Basin has been debated for almost 40 years. However, the latest research suggested that the Cambrian source rocks, especially the Yuertusi Formation, are the major contributor to the deep marine oils, suggesting the Cambrian strata to be promising targets for future explorations (Feng et al., 2021). Based on the new findings about oil sources, PetroChina deployed a pilot well, Xiongtan 1 (XT 1), on the Kalayuergun structural belt in the western Tabei area in 2022 where in September 2023, it achieved industrial oil flow in the Upper Cambrian Xiaqiulitage Formation (Wang, 2024). This discovery, which followed previous successful explorations in the Cretaceous and Paleogene strata made the Tabei area a "multilayer oil producing reservoir" (Wang, 2024). This well is currently the only one that has achieved a breakthrough in the Cambrian strata in the Tabei area, with daily oil production of 201 t and gas of 177899 m^3 (Wang, 2024). Considering this, it is necessary and urgent to further investigate oil accumulation history in this particular well and the one in its vicinity for better future exploration and development operations in the area.

Based on what was said above, the main objective of this study is investigating the oil charging history in the Xiaqiulitage Formation in the Kalayuergun structural belt by integrating fluid inclusion and carbonate U–Pb dating methods. The results can provide more discussions in the long-standing ambiguities in the use of fluid inclusions to solve the number of oil charging events and provide insight to the oil accumulation and preservation mechanisms in this promising frontier area.

2. Geological setting

The Tarim Basin is the largest superimposed petroleum-bearing basin in China (Zhang et al., 2015). It is located in the northwest of China, covering an area of about 560 $\times$ 10^3 km^2 (Fig. 1(a)) (Zhu et al., 2013). The Tarim Basin is tectonically located between the Paleo-Asian and Tethyan tectonic domains (Zhu et al., 2019). The basin is bounded by the Kunlun Mountains to the southwest, the Tianshan Mountains to the north, and the Altun fault belt to the southeast (Cheng et al., 2020; Lin et al., 2012). Within the basin, it can be divided into the Luntai, Lunnan, Yingmaiti, Bachu, Tazhong, Southeastern and Wensu-Keping uplifts, and the Awati, Kuqa, Manjiaer, Tangguzibasi, southwestern and southeastern depressions, et al. (Fig. 1(b)) (Cheng et al., 2020). Since the Mesoproterozoic collision that formed its crystalline basement, the Tarim Basin has experienced multiple stages of tectonic movements, including the early Caledonian extension with the development of carbonate successions (Jia et al., 2022), the middle-late Caledonian to early Hercynian compression that resulted in the formation of sub-structural units in the Tarim craton (Yang et al., 2014; Zhu et al., 2019). The late Hercynian-Indosinian compression facilitated the formation of the Tabei Uplift (Jia et al., 2022), which was later affected by the late Yanshanian compression and the late Himalayan tectonic deformation (Zeng et al., 2004). The Kalayuergun structural belt is located at the western part of the

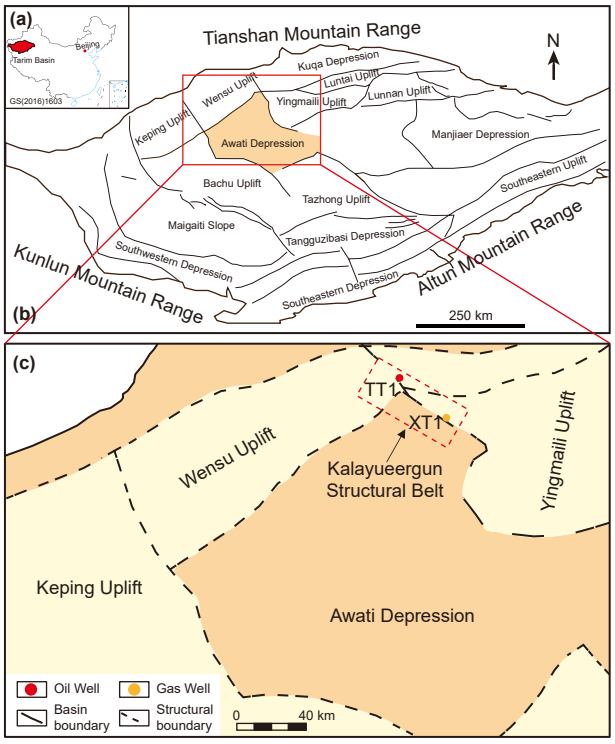

Fig. 1. Locations of the Tarim Basin (**a**) and the study area (**b**), and the geological map of the study area (**c**).

Tabei Uplift, which is bounded by the Qiulitage structural belt to the northeast, and the Awati Depression and Wensu Uplift to the southwest (Fig. 1(c)) (Wang, 2024). It is characterized by en-echelon folds containing the northern, middle and southern Kalayuergun anticlines (Zhang et al., 2018).

The stratigraphy of the Tarim Basin is comprised of the Sinian–Devonian marine deposits, the Carboniferous–Permian transitional deposits, and the Triassic–Quaternary continental deposits (Fig. 2) (Zhu et al., 2019). The target wells in this study are Well XT 1 and another one in its vicinity, Well Tuotan 1 (TT 1) (Fig. 1(c)). The Well TT 1 was drilled on the Kalayuergun Structural Belt, aiming at exploring the Paleozoic burial hill reservoir domain. The Cambrian Xiaqiulitage Formation is mainly composed of dolomite grainy shoal with a thickness of 251 m in Well XT 1 and 138 m in Well TT 1. Wang (2024) divided the reservoirs of the Xiaqiulitage Formation based on their porosity as Type I and Type II, when porosity exceeds and equals to 5% or when it is less than 5%, respectively. Herein, well-log data indicates that the Xiaqiulitage Formation ($\in_3 q$ in Fig. 2) in Well XT 1 is comprised of type I reservoir of 24.7 m thick, with average porosity of 10.3%; and type II reservoir of 168 m thick, with average porosity of 5.62%. The oil producing layers have a total thickness of 96.5 m. The oil produced from Well XT 1 is characterized with density of 0.8096 g/cm^3 at 20 °C and 0.7873 g/cm^3 at 50 °C, with sulfur, wax, resin and asphaltene contents of 0.419%, 2.1%, 0.34%, and 0.09%, respectively (Wang, 2024), while the Xiaqiulitage Formation in Well TT 1 is mainly type II reservoir with thickness of 92.5 m and average porosity of 4.3%.

3. Samples and methods

3.1. Samples

Two sets of core samples, consisting of twelve and eleven samples, were collected from the Xiaqiulitage Formation from wells XT 1 and TT 1, respectively. The core samples are composed of fine, medium and coarse crystalline dolomites observable by the naked eye (Fig. 3). The core samples were cut and prepared as doubly-polished thick sections (~100 μm thick) for petrographic observations and fluid inclusion studies. All petrographic observations and geochemical examinations were carried out at the Key Laboratory of Basin Structure and Hydrocarbon Accumulation, PetroChina, Beijing, China.

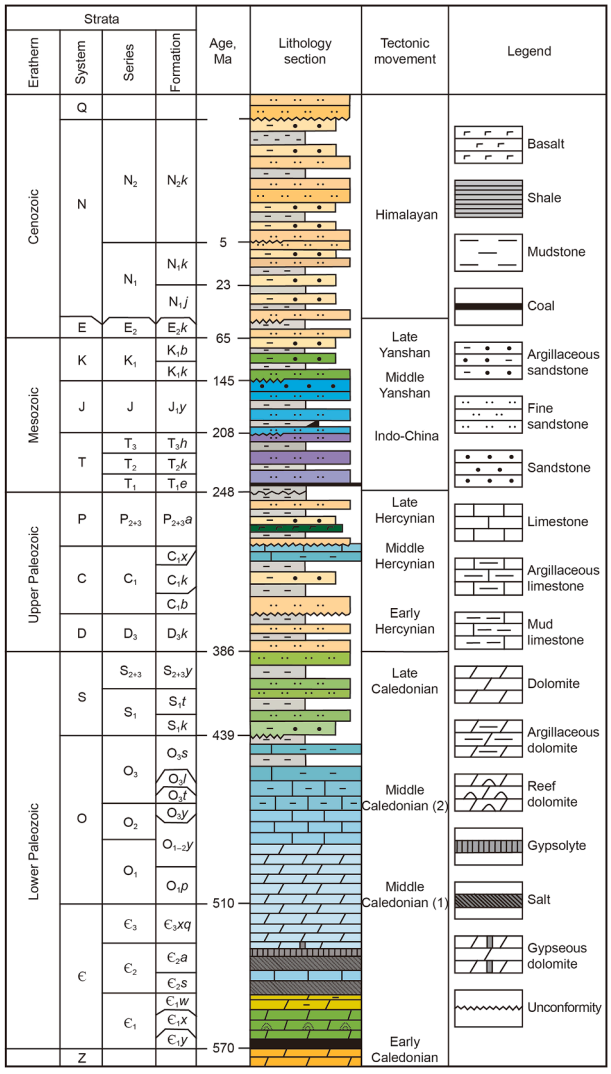

Fig. 2. Stratigraphic column of the Tarim Basin (after Zhu et al. (2019) and Yang et al. (2021a)).

3.2. Optical microscopy

A Zeiss Axio Imager M2m microscope was used for petrographic observations under transmitted light (TL) and ultraviolet light (UV) while a CLF-2 stage was employed for cold cathodoluminescence (CCL) observations (working conditions: 12.5 kV and ~555 μA).

3.3. Fluid inclusion analyses

An USB4000 micro-beam fluorescence spectrometer was utilized for acquiring fluorescence spectra of oil inclusions. The fluorescence spectral parameters λ_{max} and QF_{535} were then

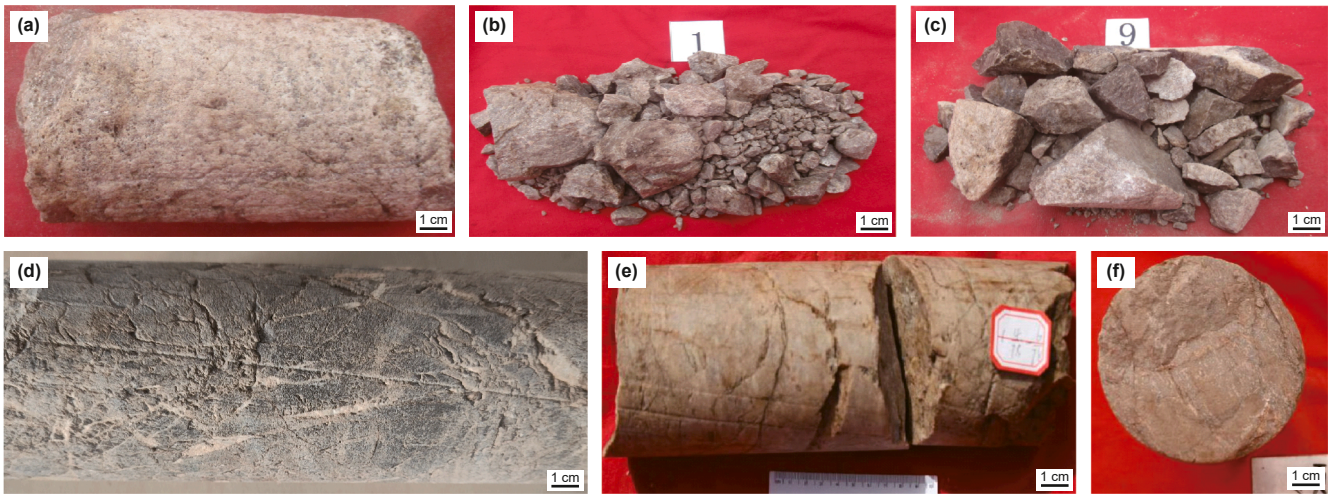

Fig. 3. Photographs of core samples from the Xiaqiulitage Formation from wells XT 1 and TT 1. (**a**), (**b**) and (**c**) Well XT 1, 6709 m, fine crystalline dolomite with severe fracturing. (**d**), (**e**) and (**f**) Well TT 1, 5688.2–5756.8 m, coarse, medium and fine crystalline dolomites.

calculated for oil inclusion compositional maturity determination. The definition of λ_{max} and QF_{535} can be found in Munz (2001) where λ_{max} is the wavelength at the maximum intensity and QF_{535} is the ratio of flux from 535 nm to 750 nm to the flux from 430 nm to 535 nm. A Linkam THMS600 heating-freezing stage, which is calibrated by synthetic fluid inclusions, is used for homogenization temperature measurements with precision estimated to be within ±0.1 °C.

3.4. Carbonate U–Pb dating

Calcite in-situ U-Pb dating was done with a Thermo Element XR and NWR 193 nm LA ICP-MS system. LA-ICP-MS in-situ calcite U–Pb dating was completed in the Key Laboratory of Basin Structure and Hydrocarbon Accumulation, PetroChina, Beijing, China, with the Thermo XR high resolution plasma mass spectrometer and the NWR 193 nm excimer laser system. The single-point ablation method was used, with a laser power of 2 J/cm^2, a pulse frequency of 10 Hz, an ablation spot of 160 μm, a laser pre-ablation time of 2 s, an ablation time of 20 s, and a purge time of 20 s. The mass spectrometer used a peak-hopping method to detect the signal intensities of ^{202}Hg, ^{204} (Hg + Pb), ^{206}Pb, ^{207}Pb, ^{208}Pb, ^{232}Th, and ^{238}U, and the time for each analysis point was 48 s. NIST614 and WC-1 were used as the test standards, while TARIM was set as the laboratory standard. NIST 614 was utilized to correct instrument signal drift and the ^{207}Pb/^{206}Pb ratio of carbonates, and WC-1 (recommended age value is 254.8 ± 6.4 Ma) was employed as the main standard to correct the ^{238}U/^{206}Pb ratio of the detection standard TARIM and the test sample. The “Trace_Element DRS” and “U–Pb Geochronology” calibration methods in Iolite V4 software were considered to calculate the element content, while the isoplot in Excel was used for plotting. In order to improve the success rate of carbonate dating, this paper followed the grid and element surface scanning preliminary screening methods to determine the denudation sample points and selected the locations where ^{238}U and ^{206}Pb were relatively high for LA-ICP-MS in-situ calcite U–Pb dating. The test age of the TARIM is 211.1 Ma (the recommended age value is 208.8 ± 0.6 Ma), which results in an experimental error of less than 2% (Lu et al., 2023; Gui et al., 2025).

3.5. 1D basin modeling

1D basin models (burial histories) of the wells XT 1 and TT 1 were reconstructed by using the Petromod software. The required input parameters, including the stratigraphy, age, depth, lithology, paleowater depth, heat flow, and measured bottom hole temperatures were referred to PetroChina's internal well reports which are still confidential documents. The modeled thermal history used the EASY%R_o model (Sweeney and Burnham, 1990).

4. Results

4.1. Petrography

The Xiaqiulitage Formation in the Well XT 1 is mainly comprised of a fine-crystalline dolomite matrix (30–100 μm maximum length) with some dolomite crystals showing a dark core and bright rim (Fig. 4(a)). Dissolution pores (400–1100 μm wide and several millimeters long) are commonly encountered in the fine crystalline dolomite matrix, with medium crystalline dolomite growing on the edge of the dissolution pores (Fig. 4(a) and (b)). Most of the dissolution pores are connected by thin open fractures (Fig. 4(b)). Healed fractures are also found in the dolomite matrix, showing dark color under TL (Fig. 4(c)). The dolomite matrix exhibits a red core and dull red rim under CCL with a scarlet rim occasionally occurring on the outer edge of the rhombohedral dolomite crystals (Fig. 4(d)). The healed fractures are observed with a relatively brighter red CCL color than the dolomite matrix (Fig. 4(d)). It can be seen that the dolomites in the healed fractures are characterized by the occasional appearance of a scarlet rim on the crystal edge (Fig. 4(d)).

The Xiaqiulitage Formation in the Well TT 1 is mainly composed of medium to coarse nearly equant anhedral dolomite (100–400 μm size), with half of the crystals displaying dark core and bright rim under TL (Fig. 4(e)). The dissolution pores and fractures are filled by calcite that is observed light red color under TL due to the staining by Alizarin red (Fig. 4(f)). Euhedral dolomite crystals (200–1400 μm size) with dark and bright zones under TL are commonly observed on the edge of the dissolution pores and fractures (Fig. 4(f) and (g)). Under CCL, the dolomite matrix mainly shows dull red with scattered red color on the crystal edges, while close to the dissolution fractures or pores, the dolomite matrix exhibit bright red color (Fig. 4(h)). The euhedral dolomite crystals show a dark core and a rim band with lighter red coloring (Fig. 4(h)). The calcite filling the center of the pore and fractures is seen as a dull orange to orange CCL color (Fig. 4(h)).

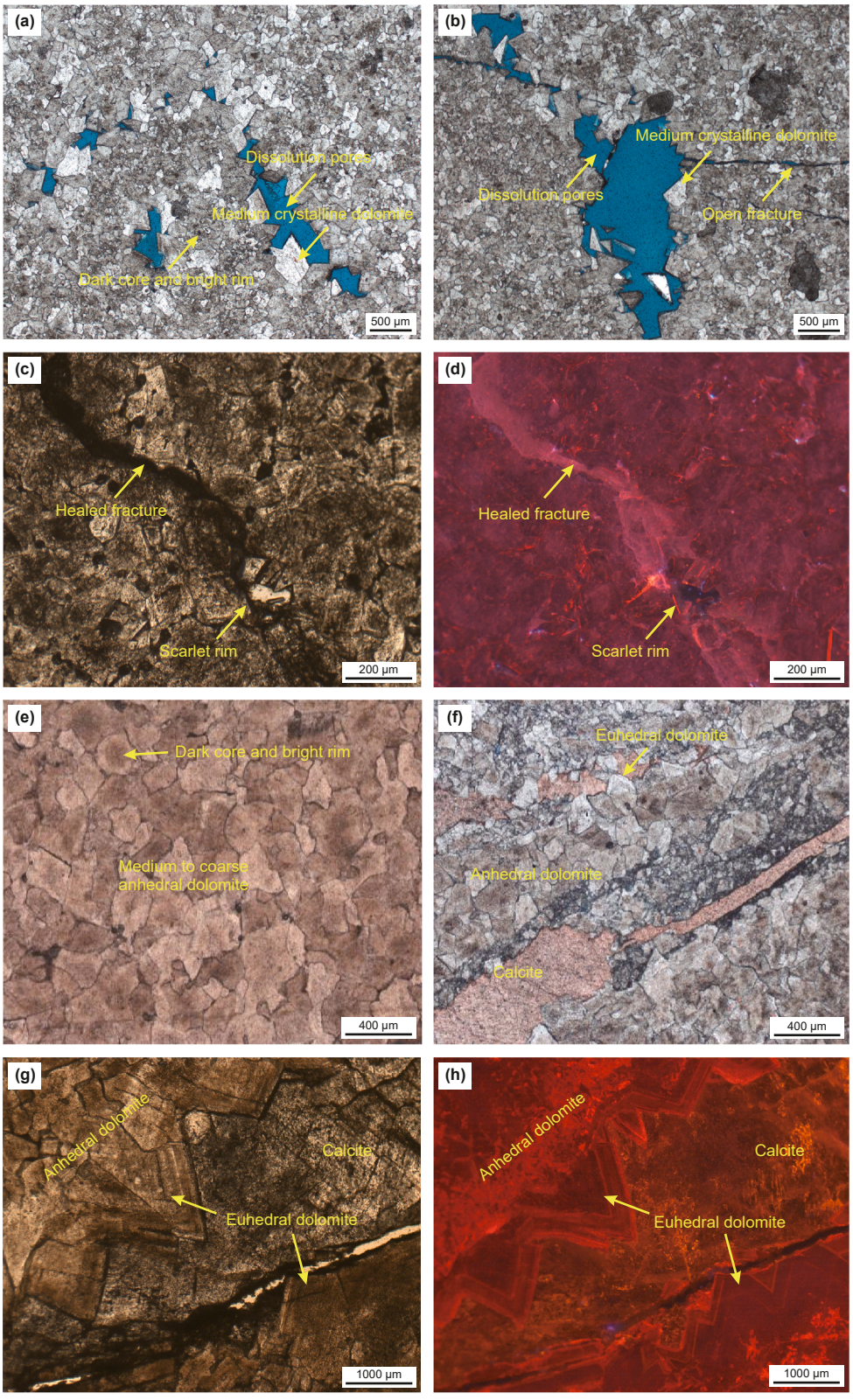

Fig. 4. Photomicrographs under the transmitted light (TL) and cold cathodoluminescence (CCL) of the Xiaqiulitage Formation in the wells XT 1 and TT 1. (**a**) and (**b**) Well XT 1, 6709 m, TL images showing dissolution pores in fine crystalline dolomite, with medium crystalline dolomite on the edge of the pores. (**c**) Well XT 1, 6709 m, TL image showing healed fracture in the dolomite matrix. (**d**) CCL image of the same field of view as (c). (**e**) and (**f**) Well TT 1, 5755.5 m, TL images showing medium to coarse anhedral dolomite matrix, with dissolution pores and fractures filled by calcite. (**g**) Well TT1, 5695.7 m, TL image showing euhedral dolomite growing on the edge of the dissolution fractures. (**h**) CCL image of the same field of view as (g).

4.2. Fluid inclusion analyses

4.2.1. Fluid inclusion petrography

Oil inclusions are found as trails cross-cutting matrix dolomite in the Well XT 1. The oil inclusions exhibit either green or blue fluorescence colors. The shapes of the inclusions are triangular or irregular, with a maximum length between 10 and 20 μm (Fig. 5(a)–(d)). Oil inclusions observed in Well TT 1 mainly are distributed in the overgrowths of calcite crystals, with the fluorescence colors including orange, yellow, green and blue (Fig. 5(e) and (f)). In addition, pure gas and coeval aqueous inclusions were also detected as clusters in calcite (Fig. 5(g) and (h)).

4.2.2. Fluorescence spectroscopy

Fluorescence spectra of the oil inclusions found in Well XT 1 are classified into two types according to their λ_{max} values (Fig. 6(a)). Accordingly, on the λ_{max} vs. QF-535 cross-plot, the data points are in two groups, with one group (λ_{max}: 515–537 nm, QF-535: 0.37–0.64) corresponding to the blue fluorescent oil inclusions and the other (λ_{max}: 564–570 nm, QF-535: 0.84–0.96) corresponding to the green fluorescent oil inclusions (Fig. 6(b)). Fluorescence spectra of oil inclusions in Well TT 1 are more complex, showing four λ_{max} positions (Fig. 6(c)). Moreover, on the cross-plot, the data points are classified into four groups, corresponding to the blue (λ_{max}: 477 nm, QF-535: 0.31), green (λ_{max}: 503–518 nm, QF-535: 0.27–0.50), yellow (λ_{max}: 529–549 nm, QF-535: 0.72–0.86) and orange (λ_{max}: 570–593 nm, QF-535: 0.67–1.34) (Fig. 6(d)).

4.2.3. Microthermometry

Homogenization temperatures of fifteen blue fluorescent oil inclusions in the same FIA in the Well XT 1 were measured, which are in a range from 85 °C to 170 °C. The histogram shows three modes, which are at around 85, 100 and 160 °C, respectively (Fig. 7(a)). The green fluorescent oil inclusion failed to obtain T_h data due to their relatively large vapor fractions. Furthermore, no coeval aqueous inclusions were found with these blue or green oil inclusions.

In Well TT 1, six blue fluorescent oil inclusions are characterized by T_h values from around 90 °C to 115 °C, with an average of 102 °C. Eight yellow fluorescent oil inclusions have T_h values from around 90 °C to 115 °C, with an average of 97 °C. Seventeen aqueous inclusions that are coeval with the blue and yellow fluorescent oil inclusions homogenized between 87 °C and 129 °C, with an average of 99 °C. The histograms do not show any mode of either the blue or yellow fluorescent oil inclusions, or their coeval aqueous inclusions (Fig. 7(b)).

4.3. Carbonate U–Pb dating

Three U–Pb ages were obtained from the samples from Well TT 1, including two ages of the dolomite matrix which are 468.3 ± 8.8 Ma (MSWD = 2.4, n = 59) and 465.5 ± 6.2 Ma (MSWD = 1.05, n = 59), respectively (Fig. 8(a) and (b)), and another age from the calcite which is 440.5 ± 9.6 Ma (MSWD = 3.7, n = 58) (Fig. 8(c)). The uranium contents of the first U–Pb age (468.3 ± 8.8 Ma) of the dolomite matrix are between 0.0518 and 2.6153 μg/g, with an average of 0.4872 μg/g. Herewith, their $^{238}U/^{206}Pb$ and $^{207}Pb/^{206}Pb$ ratios are in the range of 0.3845–13.5709 and 0.0723–0.7650, respectively. The upper intersection shows a common lead ratio ($^{207}Pb/^{206}Pb$) of 0.778. The second U–Pb age (465.5 ± 6.2 Ma) of dolomite matrix is characterized by uranium contents between 0.4496 and 3.0434 μg/g (1.3126 μg/g in average), and the $^{238}U/^{206}Pb$ and $^{207}Pb/^{206}Pb$ ratios in the range of 1.6080–12.5609 and 0.0951–0.6936, respectively, with the common lead ratio being 0.7767. The uranium contents of the calcite (440.5 ± 9.6 Ma) are in the range of 0.0303–1.7834 μg/g, with an average value of 0.2773 μg/g. The $^{238}U/^{206}Pb$ and $^{207}Pb/^{206}Pb$ ratios are from 0.3679 to 15.8427 and from 0.0569 to 0.7830, respectively, with the common lead ratio being 0.8055.

4.4. 1D basin modeling

The overall heat flow data was obtained from the internal reports of PetroChina. After the modeled thermal curve (blue line in Fig. 9(a) and (c)) was calibrated by the bottomhole temperature data (magenta round point in Fig. 9(a) and (c)), the thermal maturation and hydrocarbon generation histories of the Cambrian Yuertusi Formation are presented in Fig. 9(b) and (d). It shows that the Yuertusi source rock at the footwall reached low thermal maturity (R_o = 0.5%) in the Early Devonian (~420 Ma), medium thermal maturity (R_o = 0.7%) in the Early Permian (~280 Ma), and high thermal maturity (R_o = 1.0%) in the Early Triassic (~250 Ma). It entered the over mature stage (R_o = 1.3%) in the Paleogene (~15 Ma) and finally evolved to the present-day thermal maturity of ~2.7% R_o (Fig. 9(b)). The hydrocarbon generation history illustrates that the Yuertusi Formation had three hydrocarbon generation episodes. The first two are oil generation peaks that are during the Middle Silurian–Early Devonian (~430–400 Ma) and the Early Permian–Early Triassic (~290–250 Ma), whereas the third hydrocarbon generation episode is featured by the cogeneration of oil and gas at around 10 Ma (Fig. 9(b)). Moreover, the Yuertusi source rock at the hanging wall reached low thermal maturity in the Early Devonian (~410 Ma), medium thermal maturity in the Early Permian (~280 Ma), and high thermal maturity in the Paleogene (~5 Ma) with a present-day thermal maturity (R_o) of ~1.7% (Fig. 9(d)). The hydrocarbon generation peaks of the Yuertusi source rock at the hanging wall are the same in time as those of the source rock at the footwall (Fig. 9(d)).

5. Discussion

5.1. Origin of the oil inclusions

It is important to determine the origin of fluid inclusions before further interpretations, because it would delineate the relative time sequence between the inclusion entrapment and the host mineral growth (Roedder and Bodnar, 1980). Primary fluid inclusions are those trapped during host mineral growth, which typically appears along crystal growth zones. Whereas secondary fluid inclusions are those that are found in healed fractures, thus appearing mostly as inclusion trails in thin sections. If the trails cross-cut crystal boundary, it means that the inclusions are trapped after the termination of the growth of the host mineral; if not, the inclusions are trapped before the host mineral stops growing, thus known as pseudo-secondary fluid inclusions (Roedder, 1984).

The oil inclusions found in this study are distributed as trails that cross-cut matrix dolomite crystals in Well XT 1 (Fig. 5(a) and (b)), hence they are of secondary origin, which means that the oil inclusions were trapped after the final crystallization of the matrix dolomite. Additionally, the oil inclusions with various fluorescence colors in Well TT 1 are found along the edge of the calcite crystal boundaries (growth zones), makes them primary in origin (Fig. 5(e) and (f)), indicating that these inclusions were trapped during the calcite formation. In addition, gas inclusions were detected in the calcite crystals (Fig. 5(g) and (h)). These gas inclusions are distributed as clusters in calcite which fills the remaining space of fractures after euhedral dolomite and do not extend across crystal boundaries. Therefore, the gas inclusions in calcite are attributed to be primary in origin.

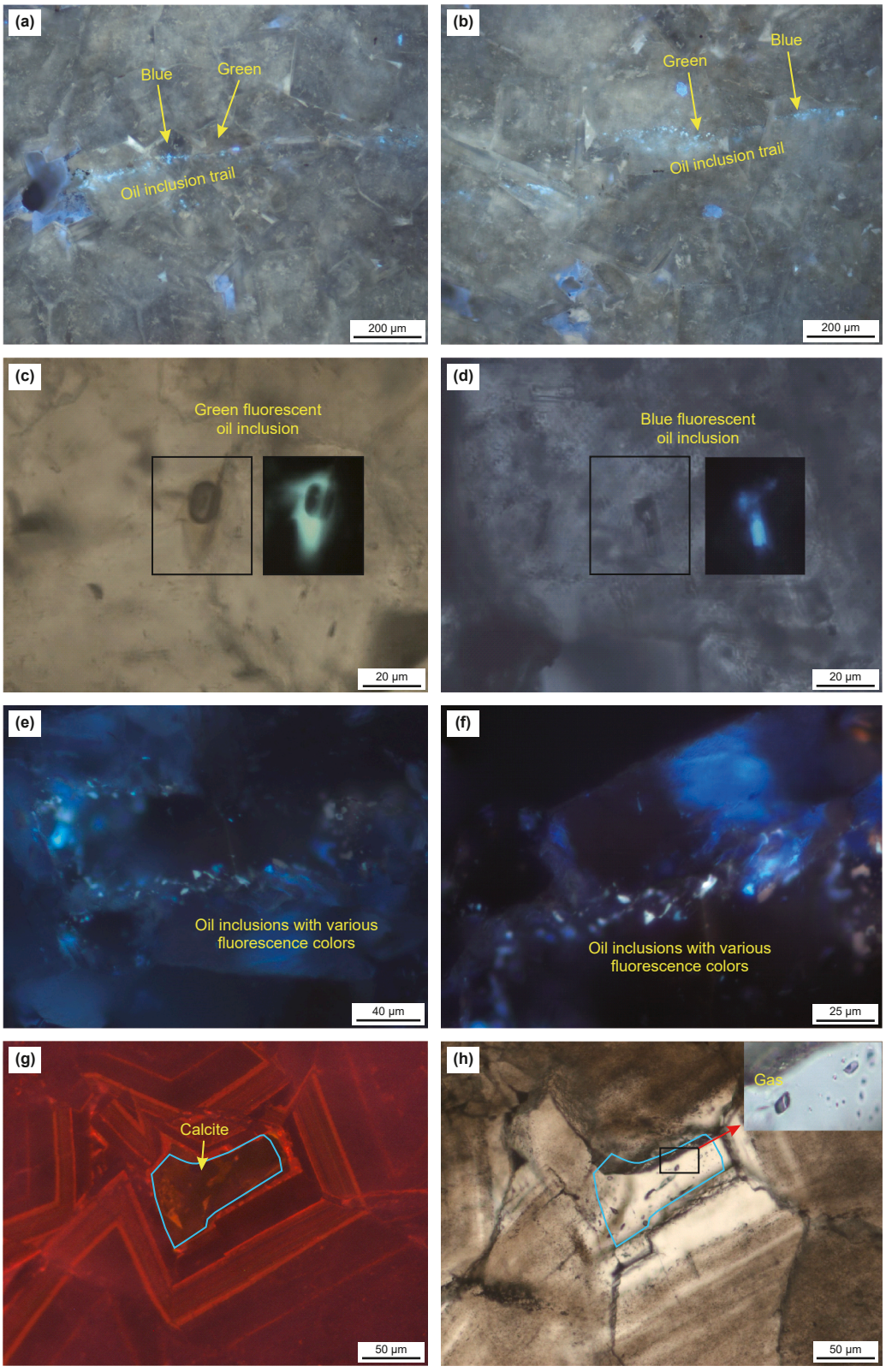

Fig. 5. Photomicrographs of oil inclusions in the dolomite crystals in the Xiaqiulitage Formation in the wells XT 1 and TT1. (**a**) and (**b**) trail of oil inclusions showing mainly green and blue fluorescence colors in the Well XT 1. (**c**) and (**d**) zoomed in pictures of single oil inclusion showing green and blue fluorescence colors, respectively, in Well XT 1. (**e**) and (**f**) oil inclusions with various fluorescence colors in calcite in Well TT 1. (**g**) CCL image of the calcite where gas inclusions were detected; (**h**) TL image showing gas and coeval aqueous inclusions in calcite.

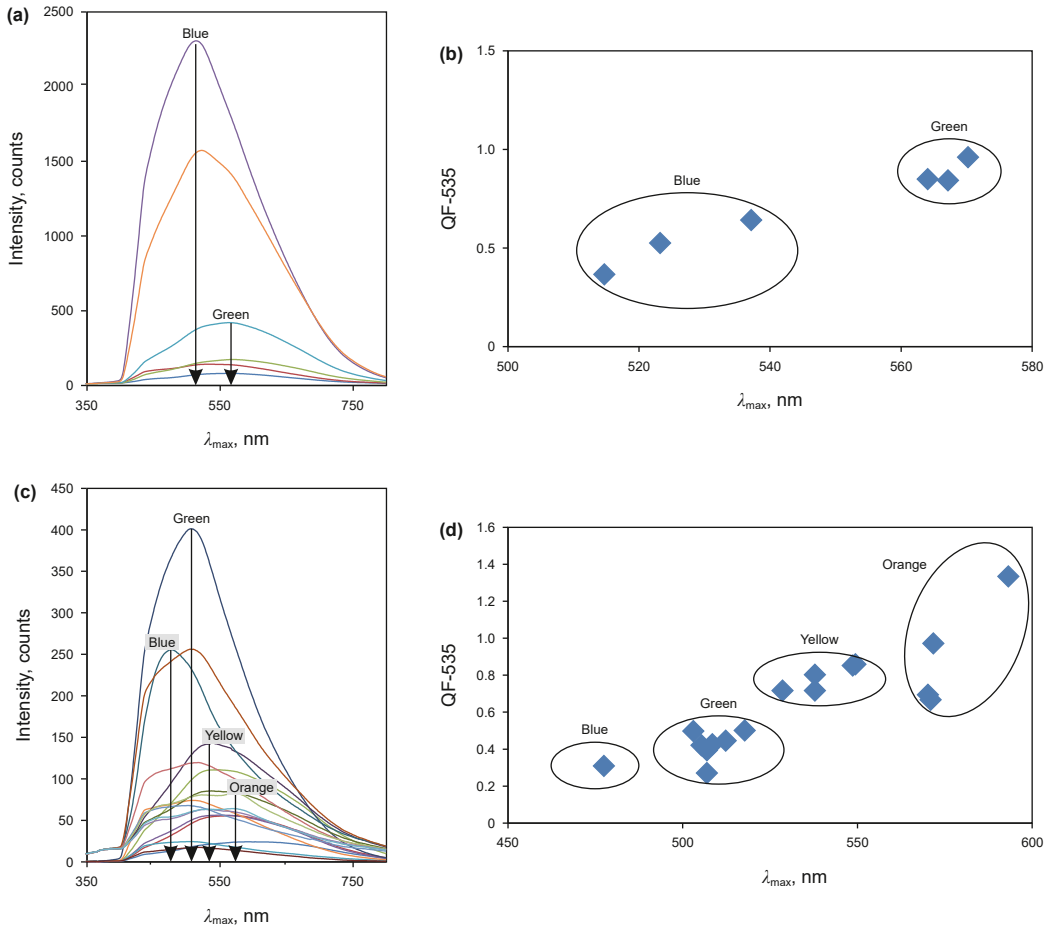

Fig. 6. Fluorescence spectra and cross-plot of fluorescence spectral parameters (λ_{max} vs. QF-535) of oil inclusions in wells XT 1 ((**a**) and (**b**)) and TT1 ((**c**) and (**d**)).

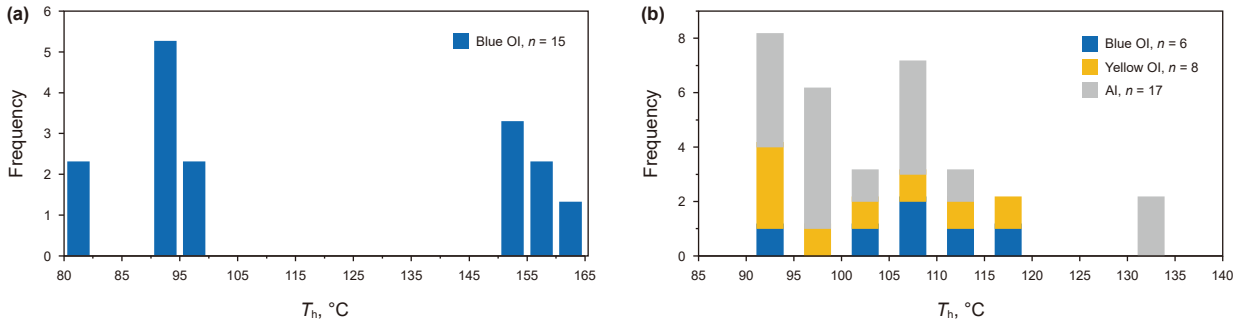

Fig. 7. Histograms of homogenization temperatures (T_h) of oil and aqueous inclusions in the Xiqiulitage Formation in the wells XT 1 (**a**) and TT 1 (**b**).

5.2. Fluorescence colors

Fluorescence colors of oil inclusions are representative of their chemical compositions which commonly are expressed as API gravity or density (Bodnar, 1990). In deep burial diagenesis, the variation of oil compositions is commonly a result of the combined temperature-time effect during the thermal maturation process of source rocks (Tissot, 1984; Tissot et al., 1974). This being said, the fluorescence colors of oil inclusions have been used to reflect their thermal maturity (Stasiuk and Snowdon, 1997). To eliminate bias introduced by the human naked eye when observations are made without the aid of a microscope, fluorescence spectral parameters were introduced to describe the fluorescence color (Munz, 2001). However, several other processes were considered also responsible for the change of oil inclusions' fluorescence colors (George et al., 2001b), and the blue fluorescent oil inclusions do not exclusively represent relatively high thermal maturity (George et al., 2001a). Synthetic oil inclusion studies have shown that the fluorescence colors of the synthesized oil inclusions are not uniform in all and have a small bias from their parent oil, which was expected to be due to the fractionation during the sample preparation process (Pironon and Pradier, 1992; Stasiuk and Snowdon, 1997). Nevertheless, such phenomenon has also been encountered in natural samples, where distinctively different fluorescent oil inclusions distribute close to each other within a single crystal which is considered to be a single trapping event, and was

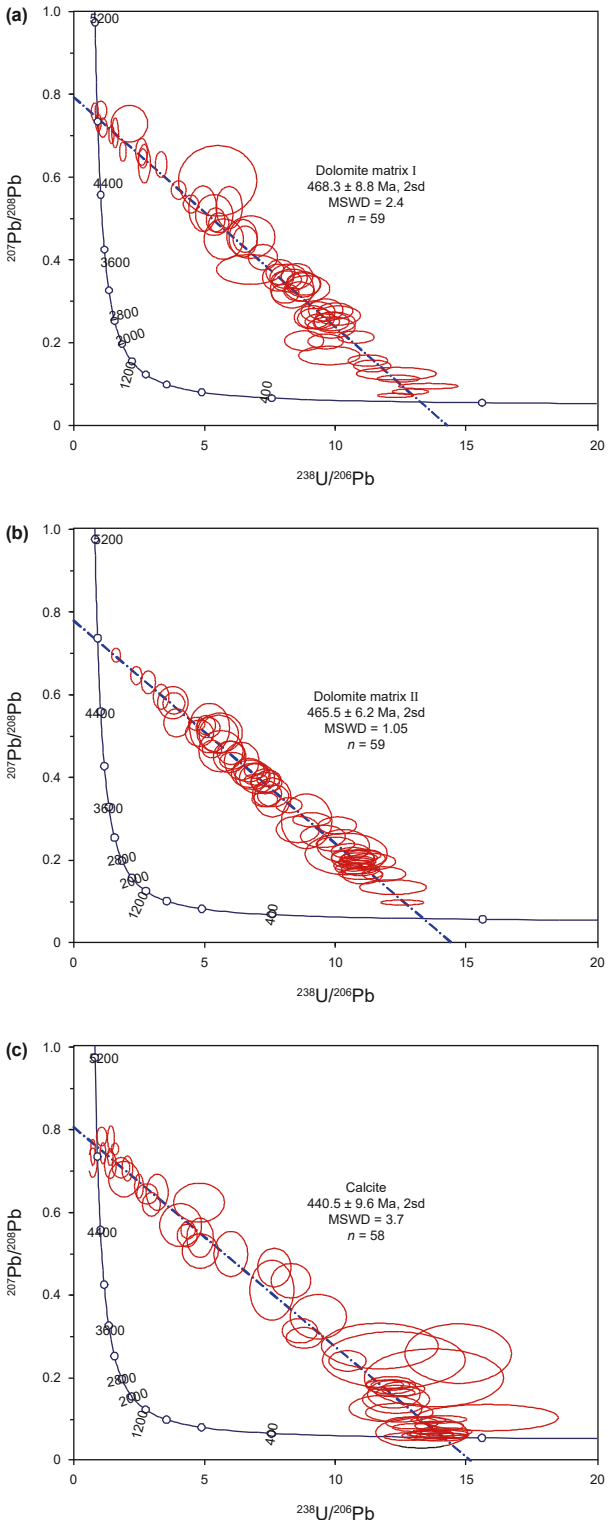

Fig. 8. U–Pb ages of the dolomite matrix ((**a**) and (**b**)) and calcite (**c**) in the Xiaqiulitage Formation in Well TT 1.

interpreted as a probable result of trapping fractionation (Pironon, 2004).

The coexistence of oil inclusions with distinctive fluorescence colors was also detected in natural rock samples (Liu et al., 2020; Ni et al., 2016; Yang et al., 2021a), indicating that the fractionation of hydrocarbon compounds may be a very common phenomenon in nature that have long been neglected. Recently, Yang et al. (2022) reported this inconsistency between fluorescence color of oil inclusions and the thermal maturity and claim that the fluorescence color is more representative of the chemical compositions. Actually, chemical compositions of oil are controlled by thermal maturation but also influenced by many other factors (Liu et al., 2024). Therefore, carefully evaluating the potential factors that may have influenced the fluorescence color of oil inclusions should be conducted before interpreting any fluorescence results (Liu et al., 2023a, 2024).

In this study, the oil inclusions with green and blue fluorescence colors in Well XT 1 are in the same healed fracture, appearing as a single trail cutting across a long distance in the dolomite matrix, indicating that the oil inclusions were trapped in a single fracturing and healing event after the formation of the dolomite matrix (Goldstein and Reynolds, 1994). Therefore, the difference in fluorescence spectral parameters could be resulted from trapping fractionation or post entrapment re-equilibrations (Fig. 6(a) and (b)). The relatively higher vapor/liquid ratio in the green fluorescent oil inclusions compared with that of the blue fluorescent oil inclusions also imply the green fluorescent oil inclusions are due to leakage after initial entrapment (Fig. 5(c) and (d)) (Pironon, 2004). Oil inclusions in calcite in Well TT 1 vary more in fluorescence colors (Fig. 5(e) and (f)). However, they distribute along the crystal growth zones, which makes them more likely to be of primary origin (Goldstein and Reynolds, 1994). Therefore, variation in the fluorescence color of these oil inclusions is also representative of either partial re-equilibration or trapping fractionation (Pironon, 2004).

5.3. T_h interpretation

In Well XT 1, no aqueous inclusions coeval with the oil inclusions were found. However, the T_h of the blue fluorescent oil inclusions shows a wide range from 85 °C to 170 °C, signifying the fluid inclusions in this FIA has potentially been altered by thermal stretching (Goldstein and Reynolds, 1994). The coeval green fluorescent oil inclusions failed to homogenize after heating due to their relatively large gas/liquid ratio, indicating the possibility of leakage and/or refilling (Goldstein, 2001). In this case, the blue fluorescent oil inclusions with relatively high T_h values resulted from re-equilibration. Therefore, the lowest T_h is representative of the highest initial trapping temperature (Rossi et al., 2002). However, no coeval aqueous inclusions were detected, thus it is unknown whether pressure correction is needed, because we don't know whether the hydrocarbon and aqueous phase are gas-saturated or not (Pironon, 2004; Roedder and Bodnar, 1980). In Well TT 1, the yellow and blue fluorescent oil inclusions yield very similar T_h ranges from ~95 °C to 115 °C. Considering the yellow and blue fluorescent oil inclusions are in the same crystal growth zone which means a simultaneous entrapment, the similarity in their T_h ranges further confirms their coeval trapping nature. The T_h range of the coeval aqueous inclusions is in the same range as that of the oil inclusions, demonstrating that the inclusion oils are gas saturated (Rossi et al., 2002). Petrographic evidence of pure gas inclusions detected in calcite can prove this interpretation (Fig. 5(g) and (h)). Therefore, no pressure correction is need for trapping temperature. Considering the T_h range of single FIA exceeds 15 °C, the minimum T_h value is expected to represent the possible trapping temperature (Rossi et al., 2002).

5.4. Timing of oil charging

Timing of oil charging is often determined by projecting the T_h values of aqueous inclusions that are coeval with oil inclusions

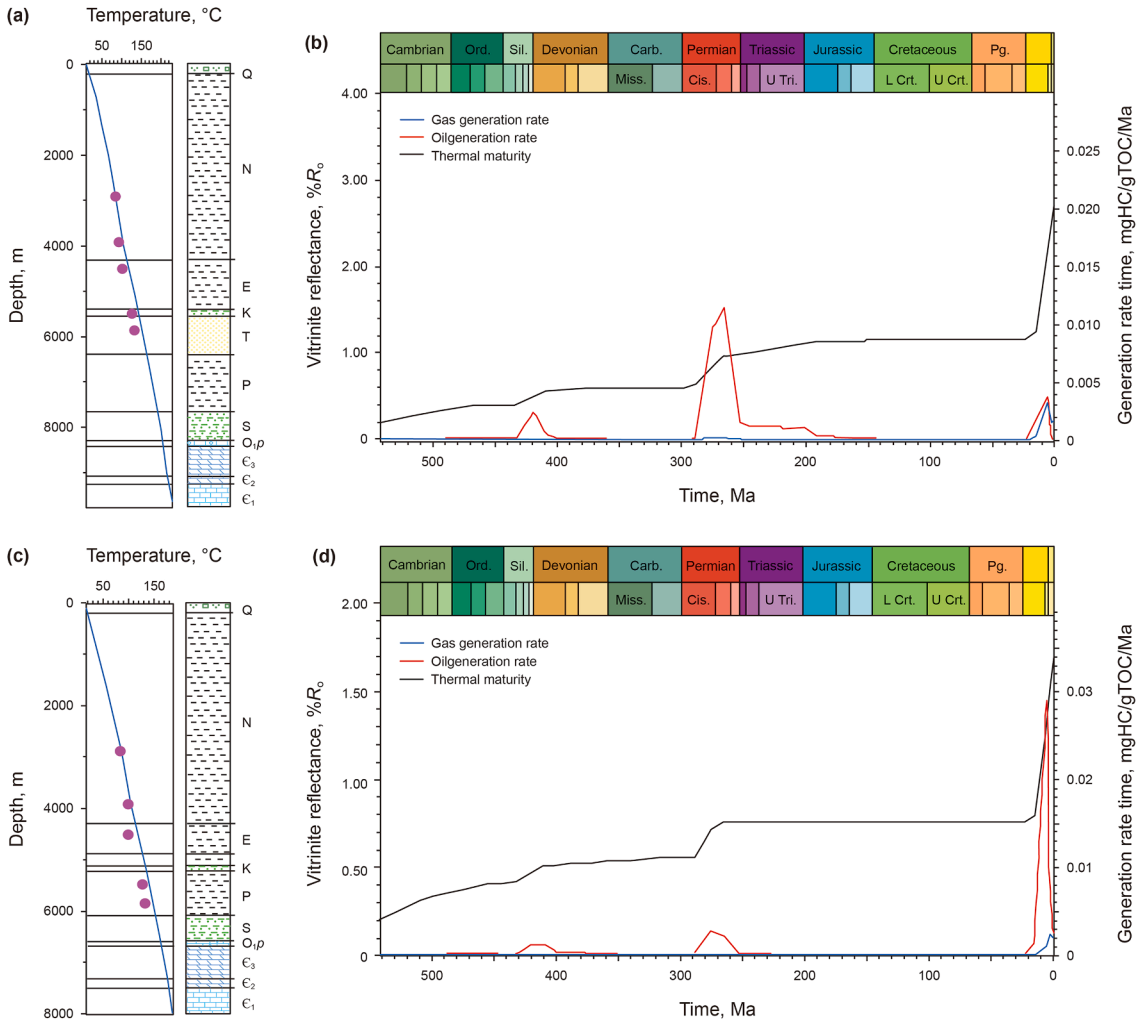

Fig. 9. Thermal and hydrocarbon generation histories of the Yuertusi Formation calculated by the 1D basin modeling. (**a**) and (**c**) Calibration profile; (**b**) and (**d**) modeled results.

onto the formation temperature-time curve calculated by 1D basin modeling (Gale et al., 2022). However, no aqueous inclusions were detected coeval with the oil inclusions in Well XT 1 and no absolute U–Pb ages were obtained from the dolomite matrix. Thus, only a relative timing that the oil inclusions postdate the matrix dolomite can be determined based on petrographic observations. The dolomite matrix in Well TT 1 yields two very similar U–Pb ages (~467–468 ± 9 Ma) (Fig. 8(a) and (b)), corresponding to the rapid burial stage (blue arrow) in the Middle Ordovician on the burial history which was calculated by 1D basin modeling (Fig. 10). These U–Pb ages are representive of the crystallization of matrix dolomite in the diagenetic history (Ni et al., 2024). However, as proceeding diagenetic alteration may alter the minerals as well as the U–Pb system, making the calculated U–Pb ages less representative of the true age of mineral formation (Godeau et al., 2018; Gui et al., 2023; Su et al., 2020). According to the petrographic observations, there is no obvious characteristics showing that the dolomite matrix underwent significant alteration such as dissolution, recrystallization (Fig. 4(c) and (d)). Besides, the calculated ratios of common Pb are near the recommended values (Fig. 8), indicating the U–Pb system is a closed system since mineral formation. Thus, the calculated U–Pb ages can represent the time of dolomite matrix formation. As discussed above, petrographic observations explain the oil inclusions in the dolomite matrix are of secondary origin (Fig. 5(a) and (b)), therefore, the timing of the oil inclusions entrapment is younger than ~455 Ma, considering an error of around 9 Ma. The oil inclusions detected in the calcite are of primary origin, denoting that the U–Pb age of calcite is representative of the age of the oil inclusions entrapment, which is 440.5 ± 9.6 Ma (Fig. 8(c)). This means a rapid burial followed by an uplifting and another rapid burial from the Later Ordovician to Early Silurian should have occurred (red arrow in Fig. 10(a)). Projecting the lowest T_h of the aqueous inclusions onto the burial history yields an age of around 450 Ma (green arrow in Fig. 10(a)), which is very close to the U–Pb age of calcite. This period is also in accordance with the first oil generation by source rock modeled by the 1D basin modeling (Fig. 9(b)). Therefore, it is inferred that the oil inclusions are representative of a very early oil charging event during the Late Ordovician to Early Silurian, corresponding to the first oil generation of the source rock of the Yuertusi Formation. As discussed above, the charged oil around crystal or grains either fractionated during mineral overgrowth and were trapped as an assemblage of inclusions with various fluorescence colors, or was subjected to reequilibration after entrapment, resulting in the chemical composition difference revealed by fluorescence color variation (Fig. 10(b)) (Liu et al., 2024).

5.5. Oil preservation mechanism

The Tarim Basin is a cold basin with low geothermal gradient (21.6 ± 2.9 °C/km at the depth interval of 0–5000 m) compared with the Sichuan Basin where early charged oil has completely

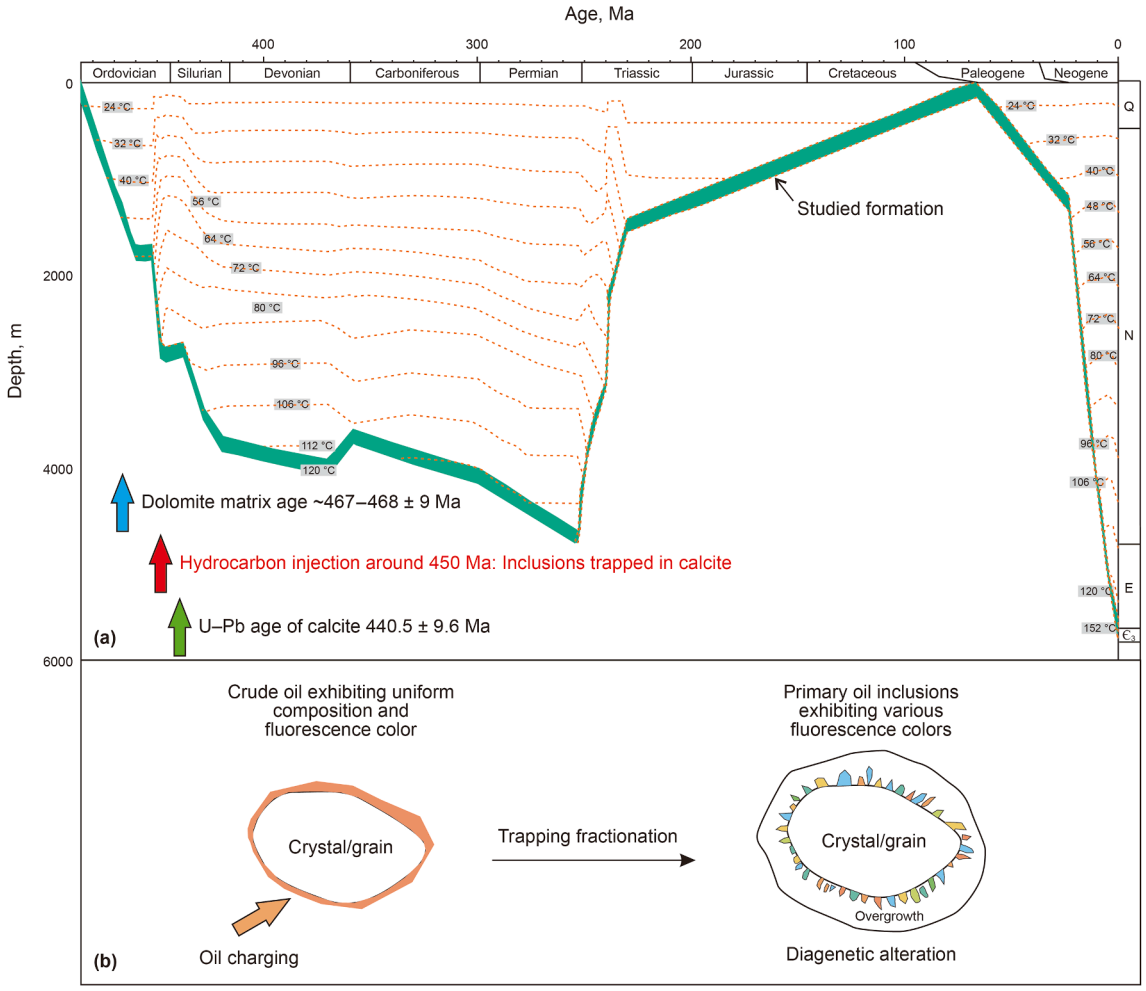

Fig. 10. (**a**) Burial history and oil charging period determination of the Xiaqiulitage Formation. (**b**) Sketch of oil trapping fractionation.

transformed into natural gas and solid bitumen (Qiu et al., 2022). The heating rate of formations after oil generation is generally about 0.9 °C/Ma in the Sichuan Basin, whereas it is only around 0.1 °C/Ma in the Tarim Basin (Qiu et al., 2022). Such low heating rate is responsible for the liquid oil preservation in the Cambrian reservoirs. According to the interpreted seismic section, the present-day burial depth of the Yuertusi Formation at the footwall is about 8200 m with a thermal maturity of ~2.7% R_o (Fig. 9(b)), while the corresponding formation at the hanging wall is buried at around 6600 m with a thermal maturity of ~1.7% R_o (Fig. 9(d)). However, the oil in the anticlinal reservoirs at around 5800 m depth is characterized by a thermal maturity of ~1.1% R_o, inferring that the burial depth is another factor that preserved the oil from thermal cracking. The difference of the thermal evolution of the Yuertusi source rocks at the footwall and hanging wall began to occur at ~435 Ma according to the maturity histories (Fig. 9(b) and (d)), denoting that the fault activity began at this time and continued to the Triassic. Assuming that the oils trapped in the fractures originate from the Yuertusi source rocks. The generated oil at around 450 Ma migrated upwards through the fault planes to the Xiaqiulitage Formation and was trapped as oil inclusions. These oil inclusions were at shallower burial depth than the Yuertusi source rocks, whereby, underwent lower thermal deformation than the source rock at the hanging wall which has a present-day thermal maturity of ~1.7% R_o. However, the trapped oils may also come from the Ordovician source rocks as previously determined oil charging time of the Ordovician strata of the Tarim Basin is very similar to the results of this study (Chang et al., 2013; Liu et al., 2003; Xiao et al., 2016). For a long time, there is a debate on the origin and main source rocks of the oil in the Tarim Basin, with geochemical correlation suggesting the oils coming from O_{2-3} source rocks while geological evidence and sulfur isotope supporting the Cambrian–O_1 source rocks as a main source (Huang et al., 2016). However, we have no evidence that can prove the oil in the inclusions was generated by Ordovician source rocks and even the oil came from the Ordovician, the results also illustrate that the shallower buried Ordovician source rock with lower thermal maturity favored the preservation of the oil. In addition, the samples in this study are restrict to two wells. Further studies about oil-source correlation in the Tarim Basin are still required. All in all, preservation of the oil inclusions as well as the later charged oils during the second and third hydrocarbon generation periods is highly plausible (Fig. 9(b) and (d)).

5.6. Implications

It has been noted that fluid inclusions in carbonate minerals are often subjected to re-equilibration after entrapment, yielding a large range of homogenization temperatures (Goldstein, 1986). However, carbonate U–Pb dating can provide absolute formation ages of diagenetic minerals, eliminating the uncertainty brought by the fluid inclusions re-equilibration and burial history

modeling. By comparing the U–Pb ages of calcite and the homogenization-burial projection results in this study, the oil charging time has been determined, which confirmed that the lowest homogenization temperature should be considered when dealing with fluid inclusions experiencing re-equilibration. China has a wide spread of carbonate reservoirs where integration of more advanced and multidisciplinary methods will make future oil/gas explorations possible.

The fluorescence colors of oil inclusions have been used as a rough indicator of the thermal maturity of the inclusion oils. Our study suggests that fluorescence color variations of oil inclusions are more indicative of compositional maturity than of thermal effects. This is because there is insufficient evidence to demonstrate that oil inclusions with different fluorescence colors, found close to each other within the same host mineral phase, were trapped at different stages of thermal maturation of the source rocks. Instead, U–Pb dating confirmed that the assumption by petrographic observations that the variation in fluorescence color of oil inclusions should have resulted from possible secondary alteration processes that changed the chemical compositions within the fluid inclusions. Therefore, when one encounters such oil inclusions assemblages in mineral crystals, a conclusion of multi-charging episodes is less likely to be drawn before exploring other supporting information, especially in deeply buried carbonate reservoirs where fluid inclusion re-equilibrations (leaking/refilling/stretching/decrepitating) are common phenomena.

Our results also imply that an insufficient time–temperature effect is responsible for the preservation of the generated oils in the deeply buried reservoirs in the Tarim Basin, even though the oils were characterized by an early charging time as revealed by U–Pb dating (~450–440 Ma) (Fig. 10). This oil charging time is very similar to that of the corresponding first oil generation and charging episode (~425 Ma) in the Cambrian Longwangmiao reservoir in the Sichuan Basin (Liu et al., 2023b; Xiao et al., 2022). However, the Sichuan Basin was subjected to a thermal anomaly caused by the Emeishan volcanic activity during the Middle Permian (~250 Ma), which induced all existing oil in-situ cracking, while the Tarim Basin is characterized by a low thermal gradient, resulting in the preservation of the oils to present-day.

6. Conclusions

This study investigated the timing of oil charging in the Xiaqiulitage Formation in the Kalayuergun structural belt by integrating fluid inclusion and carbonate U–Pb dating methods. Based on the results the following conclusions are drawn:

(1) The diagenetic sequence of the Xiaqiulitage Formation includes dolomite matrix, anhedral dolomite near fracture walls, euhedral dolomite growing towards the center of the fractures and the fracture-filling calcite.
(2) The oil inclusion trails in the dolomite matrix are of secondary origin while the oil inclusions along growth zones of calcite are of primary origin. Both types of the fluid inclusions assemblages are featured by multiple fluorescence colors, indicating potential trapping fractionation or post-entrapment alteration processes, which also suggests that although, the fluorescence color of oil inclusions is representative of inclusion oil's chemical composition, it is not always suitable as a thermal maturity indicator.
(3) The homogenization temperatures of oil inclusions with different fluorescence colors in Well TT 1 are in the same range, which further supports the coeval entrapment of the yellow and blue fluorescent oil inclusions. Considering that homogenization temperatures of oil inclusions are in the same range as those of their coeval aqueous inclusions, which indicates when the oil was trapped it has been gas saturated. This is supported by the primary gas inclusions detected in calcite.
(4) By projecting the lowest homogenization temperature of the aqueous inclusions onto the burial history model, it yields a trapping age of around 450 Ma which is very similar to the U–Pb age of calcite (440.5 ± 9.6 Ma), representing a very early oil/gas charging event during the Late Ordovician to Early Silurian, corresponding to the first oil generation of the source rock of the Yuertusi Formation. Seismic data together with thermal maturity history suggests that a low heating rate and a shallower burial depth are key factors that contribute to the preservation of the paleo liquid oils in reservoirs.
(5) This study presents a good example of using integrated carbonate U–Pb dating and fluid inclusions techniques to trace oil charging processes in deep burial reservoirs in the Tarim Basin.

CRediT authorship contribution statement

Hui Zhou: Funding acquisition. **Li-Li Gui:** Conceptualization. **Xue-Song Lu:** Resources. **Xiu-Yan Chen:** Data curation. **Yuan-Quan Zhou:** Investigation. **Xiao-Qing Yu:** Fluid inclusion thermometry. **Ying-Ying Wang:** Investigation. **Shi-Hua Yao:** Data curation. **Wen-Xia Yang:** Data curation.

Declaration of competing interest

The authors declare that they have no known competing financial interests or personal relationships that could have appeared to influence the work reported in this paper.

Acknowledgements

This study was supported by PetroChina Science and Technology Development Project (2023ZZ0206, 2021DJ0105, 2023D-5008-02, 2024-KFKT-01) and National Natural Science Foundation of China (Nos. 42472216, 42502140, 2025ZD1400402). The authors thank the efficient handling of the Editor Jie Hao and the constructive comments made by five anonymous reviewers that helped improve the quality of this manuscript.

References

Bodnar, R., 1990. Petroleum migration in the Miocene Monterey Formation, California, USA: Constraints from fluid-inclusion studies. Mineral. Mag. 54 (375), 295–304. https://doi.org/10.1180/minmag.1990.054.375.15.
Chai, Z., Chen, Z., Liu, H., Cao, Z., Cheng, B., Wu, Z., Qu, J., 2020. Light hydrocarbons and diamondoids of light oils in deep reservoirs of Shuntuoguole Low Uplift, Tarim Basin: Implication for the evaluation on thermal maturity, secondary alteration and source characteristics. Mar. Petrol. Geol. 117, 104388. https://doi.org/10.1016/j.marpetgeo.2020.104388.
Chang, X., Wang, T.G., Li, Q., Ou, G., 2013. Charging of ordovician reservoirs in the Halahatang depression (Tarim Basin, NW China) determined by oil geochemistry. J. Petrol. Geol. 36 (4), 383–398. https://doi.org/10.1111/jpg.12562.
Chen, C., Wang, Y., Beagle, J.R., Liao, L., Shi, S., Deng, R., 2019. Reconstruction of the evolution of deep fluids in light oil reservoirs in the Central Tarim Basin by using PVT simulation and basin modeling. Mar. Petrol. Geol. 107, 116–126. https://doi.org/10.1016/j.marpetgeo.2019.05.009.
Cheng, B., Liu, H., Cao, Z., Wu, X., Chen, Z., 2020. Origin of deep oil accumulations in carbonate reservoirs within the north Tarim Basin: Insights from molecular and isotopic compositions. Org. Geochem. 139, 103931. https://doi.org/10.1016/j.orggeochem.2019.103931.
Cong, F., Tian, J., Hao, F., Kylander-Clark, A.R., Pan, W., Zhang, B., 2022. Calcite U-Pb ages constrain petroleum migration pathways in tectonic complex basins. Geology 50 (6), 644–649. https://doi.org/10.1130/G49750.1.

Cong, F., Tian, J., Hao, F., Licht, A., Liu, Y., Cao, Z., Eiler, J.M., 2021. A thermal pulse induced by a Permian mantle plume in the Tarim Basin, Northwest China: constraints from clumped isotope thermometry and in situ calcite U-Pb dating. J. Geophys. Res. Solid Earth 126 (4), e2020JB020636. https://doi.org/10.1029/2020JB020636.
Cong, F., Tian, J., Hao, F., Wang, Q., Kylander-Clark, A.R., Cao, Z., 2024. In-situ calcite U-Pb ages and absolute timing of oil charge events: A case study of ultra-deep carbonate reservoirs in the Shunbei oilfield, Tarim Basin, Northwest China. J. Asian Earth Sci. 259, 105904. https://doi.org/10.1016/j.jseaes.2023.105904.
Dai, J., Zou, C., Liao, S., Dong, D., Ni, Y., Huang, J., Wu, W., Gong, D., Huang, S., Hu, G., 2014. Geochemistry of the extremely high thermal maturity Longmaxi shale gas, southern Sichuan Basin. Org. Geochem. 74, 3–12. https://doi.org/10.1016/j.orggeochem.2014.01.018.
Du, S., Hu, T., 2024. Mechanisms of hydrocarbon generation from organic matters: Theories, experiments and simulations. Adv. Geo. Energy Res. 12 (2), 156–160. https://doi.org/10.46690/ager.2024.05.07.
Eltom, H., Rankey, E., Goldstein, R., Barati, R., 2023. Passageways for permeability: Geostatistical simulation of controls on the connectivity of vug-to-vug pore networks. AAPG 107 (7), 1037–1058. https://doi.org/10.1306/04192320212.
Fan, Q., Liu, D., Du, W., Li, Y., Liang, F., Zhao, F., Feng, X., Chen, Y., Zhang, Z., Zhang, Y., 2023. In situ U-Pb dating of carbonate veins in Cambrian shales constrains fluid flow and hydrocarbon evolution at the southeastern margin of the Upper Yangtze platform, southwestern China. Geol. Soc. Am. Bull. https://doi.org/10.1130/B36893.1 (in press).
Fang, R., Li, M., Lü, H., Wang, T., Yuan, Y., Liu, Y., Ni, Z., 2017. Oil charging history and pathways of the Ordovician carbonate reservoir in the Tuoputai region, Tarim Basin, NW China. Pet. Sci. 14, 662–675. https://doi.org/10.1007/s12182-017-0196-8.
Feng, L., Guangyou, Z., Xiuxiang, L., Zhiyao, Z., Zhenghui, W., Nan, X., Tao, H., Rui, W., 2021. The disputes on the source of Paleozoic marine oil and gas and the determination of the Cambrian system as the main source rocks in Tarim Basin. Acta Pet. Sin. 42 (11), 1417–1436. https://doi.org/10.7623/syxb202111002 (in Chinese).
Gale, J., Fall, A., Yurchenko, I.A., Ali, W.A., Laubach, S.E., Eichhubl, P., Bodnar, R.J., 2022. Opening-mode fracturing and cementation during hydrocarbon generation in shale: An example from the Barnett Shale, Delaware Basin, West Texas. AAPG Bull. 106 (10), 2103–2141. https://doi.org/10.1306/01062219274.
George, S., Ruble, T., Dutkiewicz, A., 2001a. The use and abuse of fluorescence colours as maturity indicators of oil in inclusions from Australasian petroleum systems. APPEA J. 41 (1), 505–522. https://doi.org/10.1071/AJ00025.
George, S., Ruble, T., Dutkiewicz, A., Eadington, P.J., 2001b. Assessing the maturity of oil trapped in fluid inclusions using molecular geochemistry data and visually-determined fluorescence colours. Appl. Geochem. 16 (4), 451–473. https://doi.org/10.1016/S0883-2927(00)00051-2.
Godeau, N., Deschamps, P., Guihou, A., Leonide, P., Tendil, A., Gerdes, A., Hamelin, B., Girard, J.P., 2018. U-Pb dating of calcite cement and diagenetic history in microporous carbonate reservoirs: Case of the Urgonian Limestone, France. Geology 46 (3), 247–250. https://doi.org/10.1130/G39905.1.
Goldstein, R., 1986. Reequilibration of fluid inclusions in low-temperature calcium-carbonate cement. Geology 14 (9), 792–795. https://doi.org/10.1130/0091-7613(1986)14<792:rofiil>2.0.co;2.
Goldstein, R., 2001. Fluid inclusions in sedimentary and diagenetic systems. Lithos 55 (1–4), 159–193. https://doi.org/10.1016/S0024-4937(00)00044-X.
Goldstein, R., Reynolds, T., 1994. Systematics of Fluid Inclusions in Diagenetic Minerals: SPEM Short Course 31. SEPM Society for Sedimentary Geology. https://doi.org/10.2110/scn.94.31.
Gui, L., Lu, X., Wang, F., Ge, C., Jiang, L., Liu, S., Xie, W., Chen, W., Fan, J., Wu, H., 2025. An improved U-Pb dating method for carbonates via LA-SF-ICP-MS mapping and its applications. Sci. China Earth Sci. 68, 1583–1598. https://doi.org/10.1007/s11430-024-1540-6.
Gui, L., Zhuo, Q., Lu, X., Yang, W., Chen, W., Wu, H., Fan, J., He, Y., Cao, R., Yu, X., 2023. Restoration of reservoir diagenesis and hydrocarbon accumulation process by calcite in-situ U-Pb dating and fluid inclusion analysis: A case study on Cretaceous Qingshuihe Formation in Gaoquan Structure, southern Junggar Basin, NW China. Petrol. Explor. Dev. 50 (6), 1386–1397. https://doi.org/10.1016/S1876-3804(24)60474-X.
Guo, X., Hu, D., Wei, Z., Li, Y., Wei, X., 2016. Discovery and exploration of Fuling shale gas field. China Petrol. Explor. 21 (3), 1–15.
Huang, H., Zhang, S., Su, J., 2016. Palaeozoic oil–source correlation in the Tarim Basin, NW China: A review. Org. Geochem. 94, 32–46. https://doi.org/10.1016/j.orggeochem.2016.01.008.
Jackson, S., Pearson, N., Griffin, W., Belousova, E., 2004. The application of laser ablation-inductively coupled plasma-mass spectrometry to in situ U–Pb zircon geochronology. Chem. Geol. 211 (1–2), 47–69. https://doi.org/10.1016/j.chemgeo.2004.06.017.
Jia, C., Ma, D., Yuan, J., Wei, G., Yang, M., Yan, L., Tian, F., Jiang, L., 2022. Structural characteristics, formation & evolution and genetic mechanisms of strizke–slip faults in the Tarim Basin. Nat. Gas. Ind. B 9 (1), 51–62. https://doi.org/10.1016/j.ngib.2021.08.017.
Jiang, L., Dong, H., Li, Y., Zhao, W., Zhang, Y., Bo, D., 2024. Deformation characteristics and exploration potential of the West Kunlun foreland fold-and-thrust belt. Adv. Geo. Energy Res. 11 (3), 181–193. https://doi.org/10.46690/ager.2024.03.03.
Jin, Z., 2023. Hydrocarbon accumulation and resources evaluation: Recent advances and current challenges. Adv. Geo. Energy Res. 8 (1), 1–4. https://doi.org/10.46690/ager.2023.04.01.
Li, F., Lü, X., Zhu, G., Chen, J., Wang, R., Wu, Z., He, T., Xue, N., 2023. Formation and preservation of ultra-deep liquid petroleum in the Ordovician sedimentary succession in Tarim Basin during the neotectonic phase. J. Asian Earth Sci. 250, 105645. https://doi.org/10.1016/j.jseaes.2023.105645.
Lin, C., Li, H., Liu, J., 2012. Major unconformities, tectonostratigraphic framework, and evolution of the superimposed Tarim Basin, Northwest China. J. Earth Sci. 23 (4), 395–407.
Liu, D., Xiao, X., Mi, J., Li, X., Shen, J., Song, Z., Peng, P., 2003. Determination of trapping pressure and temperature of petroleum inclusions using PVT simulation software—a case study of Lower Ordovician carbonates from the Lunnan Low Uplift, Tarim Basin. Mar. Petrol. Geol. 20 (1), 29–43. https://doi.org/10.1016/S0264-8172(03)00047-3.
Liu, J., Li, Z., Wang, X., Jiang, L., Feng, Y., Wallace, M.W., 2022. Tectonic-fluid evolution of an ultra-deep carbonate reservoir in the southern Halahatang Oilfield area, Tarim Basin, NW China. Mar. Petrol. Geol. 145, 105870. https://doi.org/10.1016/j.marpetgeo.2022.105870.
Liu, S., Lei, X., Feng, C., Hao, C., 2016. Estimation of subsurface formation temperature in the Tarim Basin, northwest China: Implications for hydrocarbon generation and preservation. Int. J. Earth Sci. 105, 1329–1351. https://doi.org/10.1007/s00531-015-1253-4.
Liu, X., Barres, O., Pironon, J., Unger, M., Beck, P., Fan, J., Ostadhassan, M., 2024. Molecular fractionation of ancient organic compounds in deeply buried halite crystals. Anal. Chem. 96 (42), 16493–16498. https://doi.org/10.1021/acs.analchem.4c02956.
Liu, X., Chen, H., Fan, J., Kong, L., Mu, X., Zhang, H., Safaei-Farouji, M., Ostadhassan, M., 2023a. Relationship between fluorescence and IR parameters of oil inclusions and crude oils in the Dongpu Depression (Bohai Bay Basin, China). J. Asian Earth Sci., 105705 https://doi.org/10.1016/j.jseaes.2023.105705.
Liu, X., Chen, H., Xiao, X., Zhang, H., Xu, T., 2020. Mixing characteristics of oil inclusions with different thermal maturities in the Wenliu Uplift, Dongpu Depression, Bohai Bay Basin, North China. J. Earth Sci. 31 (6), 1251–1258. https://doi.org/10.1007/s12583-020-1356-0.
Liu, X., Fan, J., Jiang, H., Pironon, J., Chen, H., Li, C., Lu, X., Yu, X., Ostadhassan, M., 2023b. Fluid history of lower Cambrian Longwangmiao Formation in the anyue gas field (Sichuan Basin, SW China). Geoenergy Sci. Eng. 231, 212308. https://doi.org/10.1016/j.geoen.2023.212308.
Lu, X., Gui, L., Chen, W., Liu, S., Wu, S., Fan, J., Liu, Q., Sun, J., Zhang, L., Xiao, Y., 2023. Improvement of in situ LA-ICP-MS U-Pb dating method for carbonate minerals and its application in petroleum geology. Sci. China Earth Sci. 66 (12), 2914–2929. https://doi.org/10.1007/s11430-022-1072-2.
Mangenot, X., Gasparrini, M., Gerdes, A., Bonifacie, M., Rouchon, V., 2018. An emerging thermochronometer for carbonate-bearing rocks: Δ 47/(U-Pb). Geology 46 (12), 1067–1070. https://doi.org/10.1130/G45196.1.
Munz, I., 2001. Petroleum inclusions in sedimentary basins: Systematics, analytical methods and applications. Lithos 55 (1–4), 195–212. https://doi.org/10.1016/S0024-4937(00)00045-1.
Ni, Z., Wang, T., Li, M., Fang, R., Li, Q., Tao, X., Cao, W., 2016. An examination of the fluid inclusions of the well RP3-1 at the Halahatang Sag in Tarim Basin, northwest China: Implications for hydrocarbon charging time and fluid evolution. J. Petrol. Sci. Eng. 146, 326–339. https://doi.org/10.1016/j.petrol.2016.04.038.
Ni, Z., Zhao, J.-x., Feng, Y., Liu, H., Liu, F., Zhou, W., Luo, B., 2024. Geochemical, isotopic, and U–Pb geochronological constraints on multiple dolomitization and petroleum charging events in Precambrian carbonate reservoirs in the Sichuan Basin, China. Mar. Petrol. Geol. 165, 106908. https://doi.org/10.1016/j.marpetgeo.2024.106908.
Pironon, J., 2004. Fluid inclusions in petroleum environments: Analytical procedure for PTX reconstruction. Acta Petrol. Sin. 20 (6), 1333–1342.
Pironon, J., Pradier, B., 1992. Ultraviolet-fluorescence alteration of hydrocarbon fluid inclusions. Org. Geochem. 18 (4), 501–509. https://doi.org/10.1016/0146-6380(92)90113-C.
Qiu, N., Chang, J., Zhu, C., Liu, W., Zuo, Y., Xu, W., Li, D., 2022. Thermal regime of sedimentary basins in the Tarim, Upper Yangtze and North China cratons, China. Earth Sci. Rev. 224, 103884. https://doi.org/10.1016/j.earscirev.2021.103884.
Rasmussen, B., Zi, J., Muhling, J., Dunkley, D., Fischer, W., 2020. U-Pb dating of overpressure veins in late Archean shales reveals six episodes of Paleo-proterozoic deformation and fluid flow in the Pilbara craton. Geology 48 (10), 961–965. https://doi.org/10.1130/G47526.1.
Roberts, N., Rasbury, E., Parrish, R., Smith, C., Horstwood, M., Condon, D., 2017. A calcite reference material for LA-ICP-MS U-Pb geochronology. G-cubed 18 (7), 2807–2814. https://doi.org/10.1002/2016GC006784.
Roedder, E., 1984. Volume 12: Fluid Inclusions. Reviews in Mineralogy. Mineralogical Society of America, Chantilly, VA, p. 644.
Roedder, E., Bodnar, R., 1980. Geologic pressure determinations from fluid inclusion studies. Annu. Rev. Earth Planet Sci. 8 (1), 263–301. https://doi.org/10.1146/annurev.ea.08.050180.001403.
Rossi, C., Goldstein, R.H., Ceriani, A., Marfil, R., 2002. Fluid inclusions record thermal and fluid evolution in reservoir sandstones, Khatatba Formation, Western Desert, Egypt: A case for fluid injection. AAPG Bull. 86 (10), 1773–1799. https://doi.org/10.1306/61EEDD78-173E-11D7-8645000102C1865D.
Song, D., Wang, T., Li, M., Zhang, J., Ou, G., Ni, Z., Yang, F., Yang, C., 2017. Geochemistry and charge history of oils from the Yuqi area of Tarim Basin, NW China. Mar. Petrol. Geol. 79, 81–98. https://doi.org/10.1016/j.marpetgeo.2016.11.004.

Stasiuk, L., Snowdon, L., 1997. Fluorescence micro-spectrometry of synthetic and natural hydrocarbon fluid inclusions: Crude oil chemistry, density and application to petroleum migration. Appl. Geochem. 12 (3), 229–241. https://doi.org/10.1016/S0883-2927(96)00047-9.

Su, A., Chen, H., Feng, Y., Zhao, J., Nguyen, A.D., Wang, Z., Long, X., 2020. Dating and characterizing primary gas accumulation in Precambrian dolomite reservoirs, Central Sichuan Basin, China: Insights from pyrobitumen Re-Os and dolomite U-Pb geochronology. Precambr. Res. 350, 105897. https://doi.org/10.1016/j.precamres.2020.105897.

Su, A., Chen, H., Feng, Y., Zhao, J., Wang, Z., Hu, M., Jiang, H., Nguyen, A.D., 2022. In situ U-Pb dating and geochemical characterization of multi-stage dolomite cementation in the Ediacaran Dengying Formation, Central Sichuan Basin, China: Constraints on diagenetic, hydrothermal and paleo-oil filling events. Precambr. Res. 368, 106481. https://doi.org/10.1016/j.precamres.2021.106481.

Sweeney, J., Burnham, A., 1990. Evaluation of a simple model of vitrinite reflectance based on chemical kinetics. AAPG Bull. 74 (10), 1559–1570. https://doi.org/10.1306/0C9B251F-1710-11D7-8645000102C1865D.

Tissot, B., 1984. Recent advances in petroleum geochemistry applied to hydrocarbon exploration. AAPG Bull. 68 (5), 545–563. https://doi.org/10.1306/ad461336-16f7-11d7-8645000102c1865d.

Tissot, B., Durand, B., Espitalie, J., Combaz, A., 1974. Influence of nature and diagenesis of organic matter in formation of petroleum. AAPG Bull. 58 (3), 499–506. https://doi.org/10.1306/83D91425-16C7-11D7-8645000102C1865D.

Wang, Q., 2024. Breakthrough and significance of oil and gas exploration of Upper Cambrian Xiaqiulitage Formation in Kalayuergun structural belt, western Tabei uplift. Acta Pet. Sin. 45 (4), 615–628.

Xiao, X., Chen, H., Li, C., Liu, X., Wang, Z., Jiang, H., 2022. Fluid inclusion evidence for oil charge and cracking in the Cambrian Longwangmiao dolomite reservoirs of the Central Sichuan Basin, China. Geofluids 2022, 3019100. https://doi.org/10.1155/2022/3019100.

Xiao, Z., Li, M., Huang, S., Wang, T., Zhang, B., Fang, R., Zhang, K., Ni, Z., Zhao, Q., Wang, D., 2016. Source, oil charging history and filling pathways of the Ordovician carbonate reservoir in the Halahatang Oilfield, Tarim Basin, NW China. Mar. Petrol. Geol. 73, 59–71. https://doi.org/10.1016/j.marpetgeo.2016.02.026.

Xu, H., Cao, Z., Gui, L., Omosanya, K.O., Geng, F., Tao, Z., Guo, X., 2024. Petroleum accumulations in the Tarim Basin during various tectonic stages as revealed by U–Pb dating of multi-phase calcite veins in deeply buried carbonate reservoirs. Mar. Petrol. Geol. 164, 106790. https://doi.org/10.1016/j.marpetgeo.2024.106790.

Xu, Q., Qiu, N., Liu, W., Shen, A., Wang, X., 2018. Thermal evolution and maturation of sinian and Cambrian source rocks in the central Sichuan Basin, southwest China. J. Asian Earth Sci. 164, 143–158. https://doi.org/10.1016/j.jseaes.2018.06.015.

Yang, P., Liu, K., Li, Z., McInnes, B.I.A., Liu, J., 2022. Evolution of Ordovician YJ1X ultra-deep oil reservoir in the yuecan oilfield, Tarim Basin, NW China. Petrol. Explor. Dev. 49 (2), 300–312. https://doi.org/10.1016/S1876-3804(22)60025-9.

Yang, P., Liu, K., Liu, J., Yu, S., Yu, B., Hou, M., Wu, L., 2021a. Petroleum charge history of deeply buried carbonate reservoirs in the Shuntuoguole low uplift, Tarim Basin, west China. Mar. Petrol. Geol. 128, 105063. https://doi.org/10.1016/j.marpetgeo.2021.105063.

Yang, P., Wu, G., Nuriel, P., Nguyen, A.D., Chen, Y., Yang, S., Feng, Y.X., Ren, Z., Zhao, J., 2021b. In situ LA-ICPMS U-Pb dating and geochemical characterization of fault-zone calcite in the central Tarim Basin, northwest China: implications for fluid circulation and fault reactivation. Chem. Geol. 568, 120125. https://doi.org/10.1016/j.chemgeo.2021.120125.

Yang, P., Wu, G., Ren, Z., Zhou, R., Zhao, J., Zhang, L., 2020. Tectono-thermal evolution of Cambrian–Ordovician source rocks and implications for hydrocarbon generation in the eastern Tarim Basin, NW China. J. Asian Earth Sci. 194, 104267. https://doi.org/10.1016/j.jseaes.2020.104267.

Yang, X., Wang, X., Tang, H., Ding, Y., Lv, H., Liu, C., 2014. The early Hercynian paleokarstification in the block 12 of Tahe oilfield, northern Tarim Basin, China. Carbonates Evaporites 29, 251–261. https://doi.org/10.1007/s13146-013-0167-0.

Zeng, L., Tan, C., Zhang, M., 2004. Tectonic stress field and its effect on hydrocarbon migration and accumulation in Mesozoic and Cenozoic in Kuqa depression, Tarim Basin. Sci. China (Ser. D) 47 (Suppl. I II), 114–124. https://doi.org/10.1360/04zd0030.

Zhan, Z., Zou, Y., Pan, C., Sun, J., Lin, X., 2017. Origin, charging, and mixing of crude oils in the Tahe oilfield, Tarim Basin, China. Org. Geochem. 108, 18–29. https://doi.org/10.1016/j.orggeochem.2017.03.007.

Zhang, S., Huang, H., Su, J., Liu, M., 2015. Ultra-deep liquid hydrocarbon exploration potential in cratonic region of the Tarim Basin inferred from gas condensate genesis. Fuel 160, 583–595. https://doi.org/10.1016/j.fuel.2015.08.023.

Zhang, Z., Sun, J., Lü, L., Wang, W., Li, Y., 2018. Neogene paleomagnetic study of the western Baicheng Depression: Implications for the intensified deformation of Tian Shan since the latest Miocene. J. Geophys. Res. Solid Earth 123 (12), 349–10,369. https://doi.org/10.1029/2018JB016953, 10.

Zhang, Z., Zhu, G., Han, J., Sun, C., Huang, C., Li, J., Zhao, K., 2022. Genesis and preservation of the giant ultradeep Hadexun petroleum accumulation in the Tarim Basin, China. J. Petrol. Sci. Eng. 208, 109249. https://doi.org/10.1016/j.petrol.2021.109249.

Zhou, C., Yu, S., Huang, W., Zhang, H., Xiao, Z., Zeng, L., Huang, W., Pan, C., 2021. Oil maturities, mixing and charging episodes in the cratonic regions of the Tarim Basin, NW China: Insight from biomarker and diamondoid concentrations and oil bulk properties. Mar. Petrol. Geol. 126, 104903. https://doi.org/10.1016/j.marpetgeo.2021.104903.

Zhu, G., Li, J., Zhang, Z., Wang, M., Xue, N., He, T., Zhao, K., 2020. Stability and cracking threshold depth of crude oil in 8000 m ultra-deep reservoir in the Tarim Basin. Fuel 282, 118777. https://doi.org/10.1016/j.fuel.2020.118777.

Zhu, G., Milkov, A.V., Li, J., Xue, N., Chen, Y., Hu, J., Li, T., Zhang, Z., Chen, Z., 2021. Deepest oil in Asia: Characteristics of petroleum system in the Tarim Basin, China. J. Petrol. Sci. Eng. 199, 108246. https://doi.org/10.1016/j.petrol.2020.108246.

Zhu, G., Zhang, S., Liu, K., Yang, H., Zhang, B., Su, J., Zhang, Y., 2013. A well-preserved 250 million-year-old oil accumulation in the Tarim Basin, western China: Implications for hydrocarbon exploration in old and deep basins. Mar. Petrol. Geol. 43, 478–488. https://doi.org/10.1016/j.marpetgeo.2012.12.001.

Zhu, G., Zhang, Z., Zhou, X., Li, T., Han, J., Sun, C., 2019. The complexity, secondary geochemical process, genetic mechanism and distribution prediction of deep marine oil and gas in the Tarim Basin, China. Earth Sci. Rev. 198, 102930. https://doi.org/10.1016/j.earscirev.2019.102930.

Zou, C., Du, J., Xu, C., Wang, Z., Zhang, B., Wei, G., Wang, T., Yao, G., Deng, S., Liu, J., 2014. Formation, distribution, resource potential, and discovery of Sinian–Cambrian giant gas field, Sichuan Basin, SW China. Petrol. Explor. Dev. 41 (3), 306–325. https://doi.org/10.1016/S1876-3804(14)60036-7.